

Fast real-time arbitrary waveform generation using graphic processing units

Juntian Tu and Sarthak Subhankar*

*Joint Quantum Institute, National Institute of Standards and Technology
and the University of Maryland, College Park, Maryland 20742 USA*

(Dated: March 26, 2024)

Real-time Arbitrary Waveform Generation (AWG) is essential in various engineering and research applications, and often requires complex bespoke hardware and software. This paper introduces an AWG framework using an NVIDIA Graphics Processing Unit (GPU) and a commercially available high-speed Digital-to-Analog Converter (DAC) card, both running on a desktop personal computer (PC). The GPU accelerates the “embarrassingly” data parallel additive waveform synthesis framework for AWG, and the DAC reconstructs the generated waveform in the analog domain at high speed. The AWG framework is programmed using the developer-friendly Compute Unified Device Architecture (CUDA) runtime application programming interface from NVIDIA and is readily customizable, and scalable with additional parallel hardware. We present and characterize two different pathways for computing modulated radio-frequency (rf) waveforms: one pathway offers high-complexity simultaneous chirping of 1000 individual Nyquist-limited single-frequency tones for 35 ms at a sampling rate of 560 MB/s, and the other pathway allows simultaneous continuous chirping of 194 individual Nyquist-limited single-frequency tones at 100 MB/s, or 20 individual tones at 560 MB/s. This AWG framework is designed for fast on-the-fly rearrangement of a large stochastically-loaded optical tweezer array of single atoms or molecules into a defect-free array needed for quantum simulation and quantum computation applications.

I. INTRODUCTION

Arbitrary Waveform Generation (AWG) is used in a broad range of applications such as audio systems [1], computer music synthesis [2], quantum computation and quantum simulation [3–10], electronic warfare and radio systems [11], and photolithography [12], to name a few. Typically, the arbitrary waveforms are digitally generated using a Field-Programmable Gate Array (FPGA)[13, 14], or a Digital Signal Processor (DSP)[15, 16], which are then reconstructed in the analog domain via a high-speed Digital-to-Analog Converter (DAC). While these implementations offer flexibility, low-latency, high-throughput, and real-time processing capabilities, they are typically bespoke and challenging to develop [17].

High-speed AWG benefits from advanced pipelining and parallel processing, which are typically implemented on FPGA-based systems [18]. With the advent of accessible and general-purpose parallel programming on multithreaded multiprocessor architectures such as Graphics Processing Units (GPUs), accelerated AWG can also be performed on GPUs. GPUs are a high-bandwidth, high-parallelism, high-throughput, many-core processor architecture specialized for floating-point arithmetic operations [19]. GPUs are optimized for throughput rather than latency, while the opposite is true for Central Processing Units (CPUs). Unlike CPUs, which typically host dozens of cores and are optimized for the sequential execution of instructions via advanced pipelining and caching, GPUs host thousands of lightweight cores organized into multiple Streaming Multiprocessors (SMs)

that can execute thousands of threads concurrently [20–23]. Therefore, highly data parallel problems, which require minimal context switching, can be solved efficiently on GPUs. Furthermore, NVIDIA provides the Compute Unified Device Architecture (CUDA) Toolkit compatible with most of its GPU cards, which allows parallel programming on a high-level language like C/C++. Lastly, high-speed data transfers to peripherals (like a DAC) over the Peripheral Component Interconnect Express (PCIe) interface via Remote Direct Memory Access (RDMA) can be performed readily.

Recently, General Purpose GPU (GPGPU) computing has shown promise over DSPs and FPGAs in radar signal and data processing [24]. In fact, GPUs have shown better parallelism than FPGAs due to their large off-chip memory and high-speed coalesced access of that memory [25]. GPUs have also been used for digital signal processing [26–28] and software-defined radio (SDR) [29–32]. An extensive comparison between the capabilities of DSPs, FPGAs, and GPUs can be found in Ref. [17].

In this paper, we develop an AWG framework accelerated by GPGPU computing for fast on-the-fly rearrangement of a stochastically-loaded optical tweezer array of single atoms or molecules into a defect-free array. Numerous quantum computation and quantum simulation protocols start with a defect-free optical tweezer array of atoms or molecules [33–38]. An Acousto-Optic Deflector (AOD) driven with a multitone radio-frequency (rf) waveform is typically used to generate these optical tweezer arrays [6, 8–10]. In the case of a 1D optical tweezer array, each single-frequency tone in the multitone waveform maps to an individual optical tweezer. Single atoms are then loaded into these optical tweezer arrays albeit stochastically [39–42]. Therefore, rearranging these stochastically-loaded tweezer arrays requires dy-

* sarthaks@umd.edu.

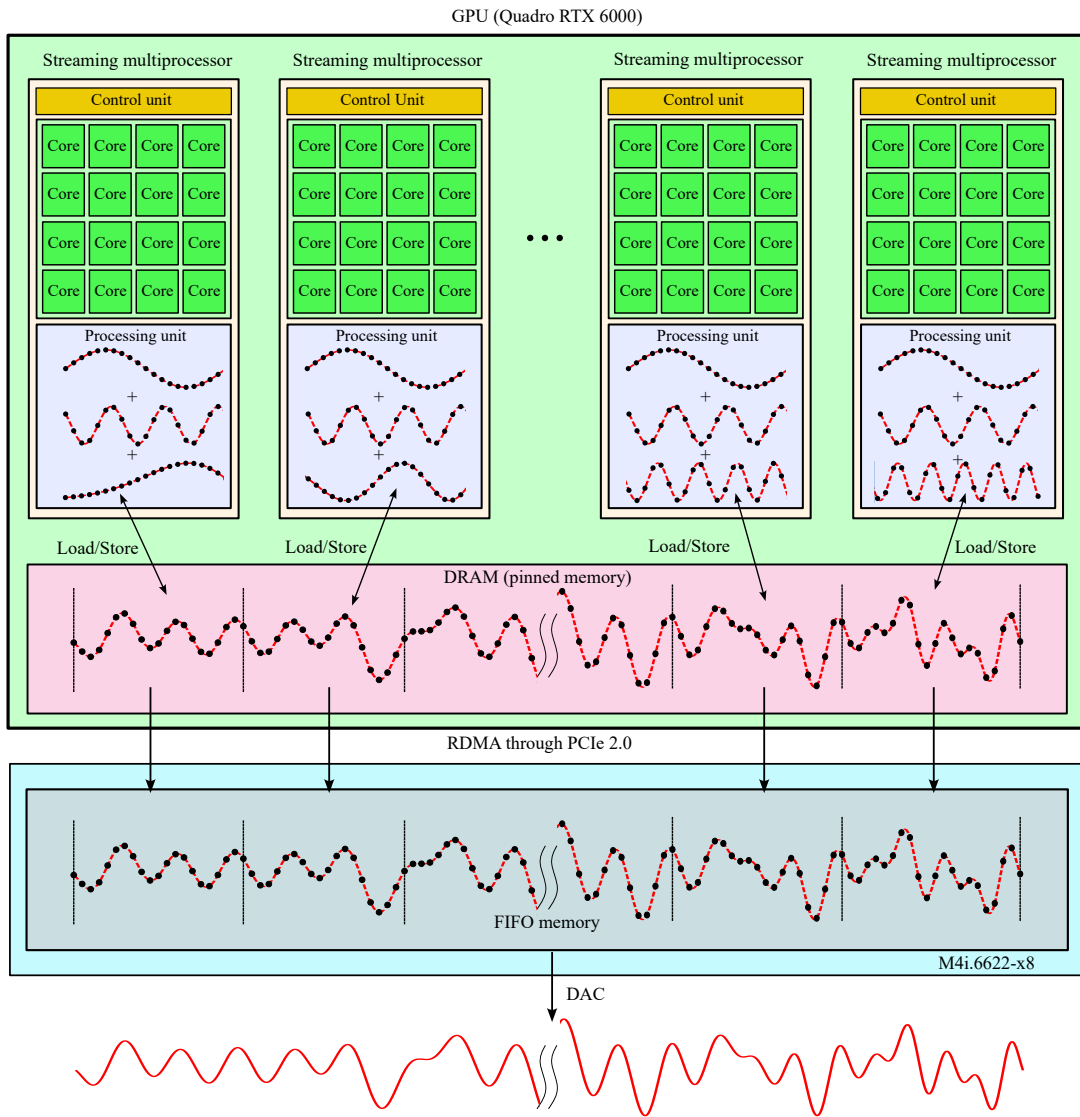


FIG. 1: Illustration of the data parallel implementation of the additive waveform synthesis framework for AWG on a GPU. Each Streaming Multiprocessor (SM) is tasked with computing and combining chunks of the wavetables to synthesize a chunk of an arbitrary waveform that is saved in the pinned memory of the GPU. This saved arbitrary waveform chunk is transferred over PCIe 2.0 via RDMA to the FIFO memory and the DAC. At the DAC, this chunk is reconstructed into an analog signal.

dynamic arbitrary control over the amplitude, frequency, and phase of the single-frequency tones that comprise the multitone waveform driving the AOD. Various groups solve this problem in clever and elegant ways. Some generate the multitone rf waveform using an FPGA-based signal generator or SDR [6, 8, 10]. Some use a PC to pre-compute and save the waveforms, and the rearrangement trajectories in memory [9, 10]. Others move an optical tweezer by controlling a voltage-controlled oscillator with a microcontroller [43].

In this paper, we cast AWG as an “embarrassingly” data parallel problem and solve it efficiently on a heterogeneous computing architecture consisting of a CPU, a GPU, and a DAC card. We synthesize static/unmodulated/continuous-wave rf waveforms

as well as real-time/dynamic rf waveforms using this architecture. Our code is portable, easy to modify, and can be found here: <https://github.com/JQIamo/AWG-on-GPU.git>.

II. THEORY OF OPERATION

Any periodic arbitrary waveform ($V(t)$) generated from a circular buffer of length L_s at a sampling clock frequency f_s can be expressed as a weighted sum of the harmonics of the fundamental frequency (f_s/L_s) via the

Fourier transform:

$$V(t) = \sum_{j=1}^N a_j \sin\left(\frac{2\pi j f_s}{L_s} t + \theta_j\right), \quad (1)$$

where a_j is the amplitude of the j th tone, θ_j is the phase of the j th tone, f_s is the sampling frequency, and N is the total number of tones. We ignore the DC term in the expansion as it is irrelevant in our application. Discretizing Eq. 1 in time we get:

$$V[i] = Q(V(t)) = \sum_{j=1}^N a_j \sin\left(\frac{2\pi j}{L_s}(i \bmod L_s) + \theta_j\right) \quad (2)$$

$$= \sum_{j=1}^N a_j x_j[i \bmod L_s] = X[i \bmod L_s], \quad (3)$$

where $t = i/f_s$ and Q is the discretization operator. Therefore, arbitrary waveform generation can be formulated as an amplitude-weighted linear combination of N wavetables (x_j) [18]. A wavetable is synonymous with the phase-amplitude lookup table in Direct Digital Frequency Synthesis (DDS). We use the phase of each tone θ_j to control for the peak/crest factor of the generated waveform $V(t)$ [44]. The formulation in Eq. 3 can be readily extended for real-time control over the spectrum of an arbitrary waveform by separating the dynamic wavetables from the static wavetables:

$$V[i] = X^{\text{static}}[i \bmod L_s] + \underbrace{\sum_j a_j x_j^{\text{dynamic}}[i]}_{X^{\text{dynamic}}[i]}. \quad (4)$$

Such a framework for control over the spectrum of an arbitrary waveform is typically referred to as additive wavetable synthesis or additive synthesis [1, 18, 45]. The additive synthesis framework laid out so far is similar to the single-phase-accumulator-type-based DDS AWG approach where a single-phase accumulator is shared between all the harmonic wavetables. The harmonics or tones are phase-locked to each other and are integer multiples of a single fundamental frequency. The harmonics are linearly combined with appropriate amplitude weights and phase shifts to generate the desired arbitrary waveform [18].

Additive synthesis frameworks with dynamic control over the phase, amplitude, and frequency chirping capabilities for each tone are typically implemented on FPGAs [18, 46, 47]. The great flexibility, low latency, and high-speed control over the spectrum afforded by an FPGA implementation should be weighed against the difficulty of the implementation [17]. On the other hand, GPU implementation of additive synthesis is much simpler. In fact, we leverage the “embarrassingly” data parallel aspects of the additive synthesis framework to accelerate AWG.

Data parallel programs run efficiently on vector processor-like architectures. This is because the same

instruction can be performed concurrently on multiple elements. This type of parallel processing architecture is referred to as Single Instruction, Multiple Data (SIMD) in Flynn’s taxonomy [20, 21]. Technically, the processing architecture on a GPU is Single Instruction, Multiple Thread (SIMT), which is different from SIMD as it does not require the lockstep execution of the threads [23]. Specifically, Eqs. 3 and 4 only require two “embarrassingly” data parallel tasks [20, 48, 49]:

- fast computation of the wavetable elements in parallel, which involves evaluating the transcendental sine function using the Special Function Units (SFU) native to the GPU, and
- vector addition of the amplitude-weighted wavetables.

Given the large gigabyte-size GPU DRAM and optimized large-scale memory accesses typically performed on a GPU [20], each wavetable x_j stores j sinusoidal cycles (Eq. 3) of phase-to-amplitude mapping for the j th tone without the need for any phase-amplitude lookup table compression or sine-wave approximations [50]. When the frequency of the j th tone is chirped (Eq. 4), x_j stores its entire chirp trajectory. Furthermore, given the analytic nature of the sine function or the chirp trajectory being computed and stored in the wavetables, chunks of the wavetables that are separated in time can be computed in parallel and out-of-order by the SMs on the GPU (see Fig. 1). The vector addition of the amplitude-weighted wavetables can also be computed in parallel in a similar fashion (see Fig. 1). In essence, the additive synthesis framework for AWG is “embarrassingly” data parallel. The generated arbitrary waveform is subsequently stored in the pinned GPU memory. From there, the data is seamlessly transferred via RDMA to the FIFO memory in real time through the PCIe bus and is then reconstructed into an analog signal by the DAC. (see Fig. 1). As memory access latencies slow down program execution, especially between the GPU memory and CPU memory in a heterogeneous computing architecture, we perform no data transfers between them. Instead, we efficiently store the computed wavetables in registers and DRAM on the GPU, facilitating rapid memory access by the cores.

III. HARDWARE IMPLEMENTATION

We implement our additive synthesis framework for AWG on an NVIDIA Quadro RTX 6000 GPU card that is connected to a Spectrum Instrumentation M4i.6622-x8 card over a PCIe bus. The GPU has a 24 GB GDDR6 DRAM and supports RDMA functionality over PCIe 3.0 bus. The M4i.6622-x8 card has four 16-bit DACs with a maximum sampling rate of 1.25 GB/s for each DAC channel, when all four channels are engaged. However, the RDMA transfer rate from the GPU pinned memory to

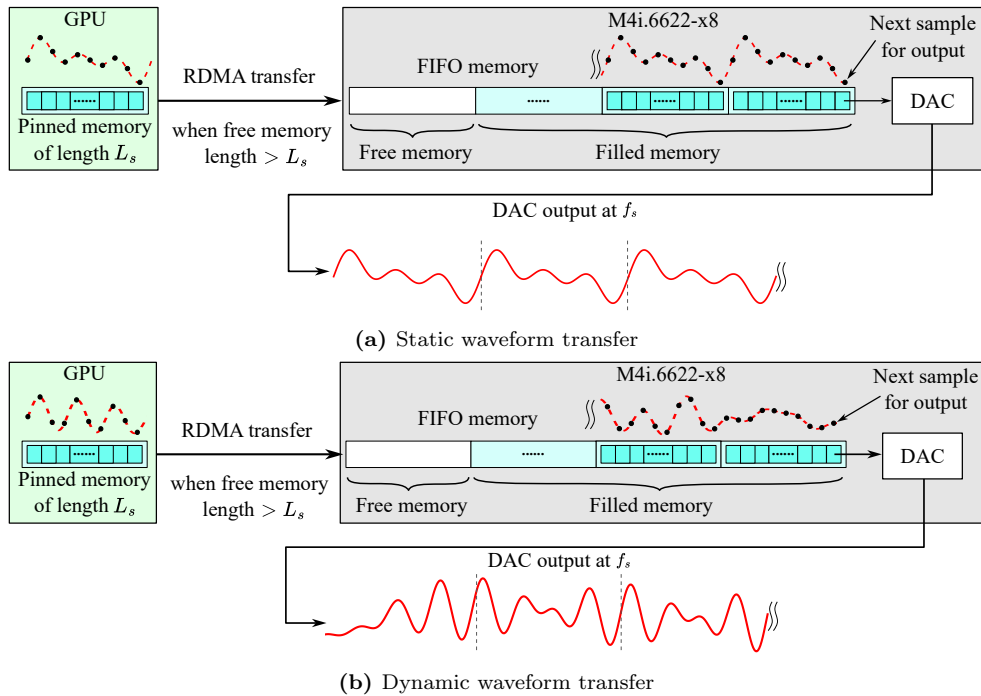


FIG. 2: Illustrating RDMA transfer between the pinned memory on the GPU and the FIFO memory on the M4i.6622-x8 card for one DAC channel. (a) The same data stored in the pinned memory is repeatedly transferred via RDMA to the FIFO memory and DAC for static AWG (b) chunks of time-varying arbitrary waveforms computed on the fly and streamed into the FIFO memory and DAC for real-time/dynamic waveform generation.

the First-In-First-Out (FIFO) memory of the M4i.6622-x8 card is limited to 2.8 GB/s as the M4i.6622-x8 card only supports RDMA transfer over PCIe 2.0. The RDMA transfer is implemented via Spectrum CUDA Access for Parallel Processing (SCAPP) SDK. The DAC sampling rate must therefore match the RDMA PCIe 2.0 transfer rate. If these two rates do not match, the FIFO buffer will be emptied (or filled) by the DAC (RDMA) before it can be refilled (or emptied) by an RDMA transfer (DAC) and a buffer underflow (or overflow) error will occur. Therefore, when all four DAC channels are engaged, the maximum sampling rate f_s achievable is 700 MB/s per DAC channel.

The optimal size of the data (or chunk) for an RDMA transfer from the pinned memory to the FIFO memory sets the lengths of all the wavetable buffers x_j and the pinned memory buffer to positive integer multiples of a minimum length L_s . In fact, the size of this chunk is 2 MiB, which implies 2^{20} samples per RDMA transfer. One sample is 2 bytes each as set by the DAC resolution. When all four DAC channels are engaged, this 2 MiB RDMA chunk is multiplexed into four 0.5 MiB sub-chunks, with one sub-chunk per DAC channel per RDMA transfer. This implies an $L_s = 2^{18}$ per DAC channel per RDMA transfer. For the sake of simplicity, we will elaborate on the additive synthesis framework with only one DAC channel in mind. We present details on how to send generated arbitrary waveform data to all four DAC channels over RDMA in Sec. IV C.

An RDMA transfer from the pinned memory to the FIFO memory is automatically invoked when the free memory length in the FIFO queue is greater than L_s . In order to avoid undesired spurs in the spectrum of the arbitrary waveform, continuous differentiability of the waveform must be enforced at the boundaries of the wavetable chunks. This is especially critical when generating a static arbitrary waveform, as it is evaluated only once and then saved in the pinned memory buffer before being fed repeatedly into the FIFO queue via RDMA (see Fig. 2a). This continuous differentiability requirement enforces a quantization on the frequency (f_j) of a single tone that can be represented by a wavetable buffer. For a DAC sampling frequency f_s , the frequency of a single tone f_j that can be stored in (and reconstructed from) a wavetable buffer x_j is

$$f_j = \frac{j}{L_s} f_s, \quad (5)$$

where $j \in \{1, 2, 3 \dots L_s/2\} \subset \mathbb{N}$ is the number of full sinusoidal cycles that can be accommodated in the wavetable buffer x_j . Any arbitrary waveform can be created by linear superposition of these amplitude-weighted and phase-shifted single-frequency tones/wavetables under the additive synthesis framework. In the next section, we elaborate on how the additive synthesis framework is implemented in software.

IV. SOFTWARE IMPLEMENTATION

This section elaborates on the waveform generation pathways that we implemented under the additive waveform synthesis framework. One pathway is devised for generating static/unmodulated/continuous-wave arbitrary waveforms (see Sec. IV A), and two pathways are devised for generating dynamic/real-time arbitrary waveforms (see Sec. IV B). A flow-chart representing the control flow of the software is shown in Fig. 3.

All pathways share a common Initialization (Init) state in which the system resets the GPU, configures the M4i.6622-x8 card, and allocates the memory for the wavetable buffers x_j in the GPU DRAM. We first layout the mathematics and the software implementation for generating static/unmodulated arbitrary waveforms and then expound on the same for generating real-time/dynamic arbitrary waveforms.

A. Static AWG pathway

Generating an static/unmodulated/continuous-wave arbitrary waveform is simple to implement under the additive synthesis framework. Any arbitrary waveform can be expressed as a linear superposition of amplitude-weighted and phase-shifted single-frequency tone wavetables. In our implementation for each DAC channel output, we set the length of all wavetable buffers and the pinned memory buffer to L_s . Therefore, a tone at a desired frequency f_0 must be approximated to its closest quantized frequency f_j as follows:

$$f_j = \frac{j}{L_s} f_s = \text{nint} \left(\frac{f_0}{f_s} L_s \right) \frac{f_s}{L_s}, \quad (6)$$

where $\text{nint}()$ denotes the operation of rounding a real number to its nearest integer. With a DAC sampling rate of $f_s = 560$ MB/s limited by the PCIe 2.0 bus, the error in this approximation is less than 534 Hz.

For a desired static arbitrary waveform $V_{\text{static}}(t)$, the digitized data ($V_{\text{static}}[i] = Q(V_{\text{static}}(t))$) in the pinned memory buffer is therefore the equation presented in Eq. 2 and 3, which we repeat here:

$$\begin{aligned} V_{\text{static}}[i \bmod L_s] &= \sum_{j=1}^N a_j x_j [i \bmod L_s] \\ &= \sum_{j=1}^N a_j \sin \left(2\pi \frac{f_j}{f_s} (i \bmod L_s) + \theta_j \right), \end{aligned} \quad (7)$$

$$(8)$$

where $t = i/f_s$, $i \bmod L_s$ denotes the array index for the wavetable buffers as well as the pinned memory buffers of length L_s for a DAC channel, and θ_j is the phase offset for the j th tone for crest/peak factor suppression [44, 51]. θ_j depends on the value of a_j [51].

One can immediately notice the benefit of this construction. The static arbitrary waveform is evaluated only once and then saved to the pinned memory buffer. By repeatedly transferring the saved wavetable in the pinned memory buffer over to the FIFO queue via RDMA, we generate a periodic static arbitrary waveform at the DAC. In our application, such a static arbitrary waveform is used to drive an AOD to create a static optical tweezer array for trapping single atoms. It is therefore essential to suppress the crest factor using θ_j , when a static rf arbitrary waveform is used to drive AODs. Prominent crest factors lead to large spikes in rf power that can damage the AOD crystal [52].

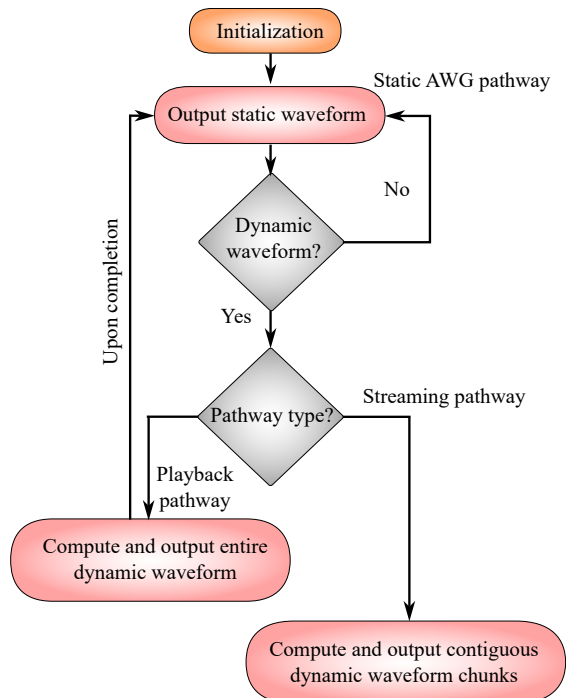


FIG. 3: Three pathways are available to the user as shown in the flowchart: static/unmodulated/continuous-wave AWG or real-time/dynamic AWG. Both the Playback pathway and Streaming pathway are available for real-time/dynamic AWG. The Playback pathway can generate highly complex real-time/dynamic arbitrary waveforms albeit for a short duration of time. This pathway terminates with a final/desired static arbitrary waveform state. The Streaming pathway allows for continuous albeit limited control over the spectrum of the arbitrary waveform for any duration of time.

B. Dynamic AWG pathways

We implement two variants/pathways for real-time/dynamic waveform synthesis. In what we call the “Playback” pathway, the entire real-time waveform is computed and saved to the pinned memory buffer prior to transferring it to the FIFO memory via RDMA and then to the DAC. This pathway enables complete control over

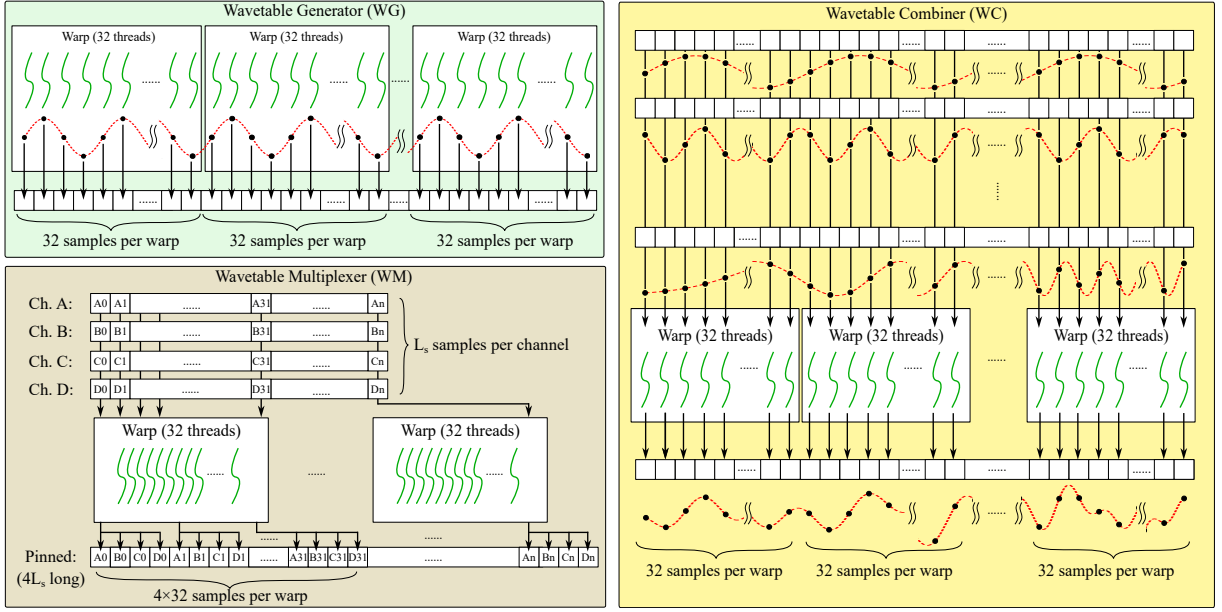


FIG. 4: The depiction of the kernel functions: In the Wavetable Generator (WG) kernel, each thread samples and evaluates a point from the analytic mathematical expression for a tone (like a sine or a chirp) and saves it to the tone’s wavetable buffer; the Wavetable Combiner (WC) vector-adds the wavetables generated by the WG; the Wavetable Multiplexer (WM) restructures the arbitrary waveform data for the four DAC channels so that each DAC channel can reconstruct its own arbitrary waveform data.

the spectrum of an arbitrary waveform for a brief period of time, facilitating a highly complex transformation of an initial static arbitrary waveform state to a desired final static arbitrary waveform state. For instance, a static array of stochastically-loaded atoms in optical tweezers can be re-arranged into a defect-free static array of atoms in optical tweezers using this pathway. As the calculation is performed on the GPU in real-time, there’s a latency/delay between the start of the computation and when the DAC is ready to output the computed real-time arbitrary waveform. The more complex the real-time arbitrary waveform, the greater is this delay.

The other pathway is called the “Streaming” pathway. In this pathway, each subsequent waveform chunk is evaluated in the time interval between the current and upcoming RDMA transfers. This allows for continuous streaming of the real-time arbitrary waveform. The waveform chunk computation must be performed faster than the time it takes to perform an RDMA transfer. While one can slow down the rate at which RDMA is performed, the Nyquist frequency is also reduced proportionally. Large Nyquist frequencies require fast computations, and this limits control over the spectrum of the arbitrary waveform to only a few tones at a time. However, unlike the Playback pathway, the Streaming pathway doesn’t have to terminate at a final static arbitrary waveform state. The performance of the two pathways will be elaborated in Section V.

The mathematics for computing the real-time/dynamic arbitrary waveform ($V_{\text{dynamic}}(t)$) is the same for both pathways. The real-time digitized

arbitrary waveform ($V_{\text{dynamic}}[i] = Q(V_{\text{dynamic}}(t))$) can be expressed under the additive synthesis framework as:

$$V_{\text{dynamic}}[i] = X^{\text{static}}[i \bmod L_s] + \underbrace{\sum_j a_j[i] \sin(\phi_j[i] + \theta_j)}_{X^{\text{dynamic}}[i]}, \quad (9)$$

where θ_j is the phase offset propagated from the initial static tone, $\phi[i]$ is the phase as a function of time during the real-time AWG. Notice the $i \bmod L_s$ indexing of only the static arbitrary waveform buffer X^{static} , but i indexing of the dynamic waveform buffer X^{dynamic} . This is because the length of the dynamic waveform buffer ($X^{\text{dynamic}}[i]$) L_d must be a positive integer multiple of L_s i.e. $L_d = L_s \left\lceil \frac{Tf_s}{L_s} \right\rceil \geq L_s$, where T is the time duration for the real-time arbitrary waveform generation.

Let’s consider the case of a real-time AWG where we only chirp the frequencies of a few tones in the spectrum of the arbitrary waveform. In this case, $a_j[i] = a_j[0]$. While we can readily program any functional form for a frequency chirp (such as linear, exponential), here we will consider the case of a frequency chirp that follows the minimum jerk trajectory [53]. The minimum jerk trajectory is typically used to minimize the heating of atoms trapped in optical tweezers during the rearrangement process. The phase of the j th tone $\phi_j[i]$ as a func-

tion of time can be expressed as follows:

$$\phi_j[i] = \begin{cases} \frac{2\pi i}{f_s} (f_j^{\text{start}} + p(i)) & i \leq T f_s \\ 2\pi \frac{f_j^{\text{finish}}}{f_s} i + \pi T (f_j^{\text{start}} - f_j^{\text{finish}}) & T f_s < i \leq L_d \\ 2\pi \frac{f_j^{\text{start}}}{f_s} (i \bmod L_s) + \theta'_j & i > L_d \end{cases} \quad (10)$$

$$\text{where } \theta'_j = 2\pi \frac{f_j^{\text{finish}}}{f_s} L_d + \pi T (f_j^{\text{start}} - f_j^{\text{finish}}) \quad \text{and}$$

$$p(i) = (f_j^{\text{finish}} - f_j^{\text{start}}) \left(\frac{5}{2} \left(\frac{i}{T f_s} \right)^4 - 3 \left(\frac{i}{T f_s} \right)^5 + \left(\frac{i}{T f_s} \right)^6 \right)$$

for the minimum jerk trajectory. In this example, the dynamic waveform generation ends in an arbitrary waveform state that is static/unmodulated/continuous-wave and is, therefore, more representative of the Playback pathway.

C. CUDA kernel implementations

The waveform synthesis pathways are implemented using CUDA kernel functions, or simply kernels, which are user-defined functions executed by the SMs on GPUs. CUDA kernels are executed in 32-thread groups called warps. A warp is the smallest unit of execution on a GPU. Multiple warps are grouped together into blocks, which are then assigned to the SMs for execution [20].

All 32 threads in a warp share a common instruction register, but process on different data. This is the SIMT parallel programming architecture. Furthermore, each thread in a warp has its own set of registers in addition to its local memory and additional memory that it shares with other threads in the warp called shared memory. In order to achieve massive speedup through data parallelism, the data should ideally be divided into warp-sized groups of 32, where each thread works on one piece of data independently. It also helps greatly if there are no control divergences in the warp. These best practices are easily satisfied in our case as the length of all the buffers is a positive integer multiple of $L_s = 2^{18}$, which is a multiple of 32, and there are no control divergences in our kernel implementations [20]. We have implemented several other strategies to speed up the code performance, which can be found in the Appendix.

There are three types of CUDA kernels implemented in the program: Wavetable Generator (WG), Wavetable Combiner (WC), and Wavetable Multiplexer (WM) as illustrated in Fig. 4. All kernels are designed to launch L_s threads that are indexed from 0 to $L_s - 1$. The number of threads is orders of magnitude greater than the number of available cores. This helps increase GPU throughput via latency hiding by assigning multiple thread blocks per SM.

The WG kernel computes the wavetables x_j . A wavetable can hold either a single-frequency tone (see Sec. IV A) or the entire chirp trajectory of a tone (Sec. IV B). For generating N single-frequency tone wavetables of length L_s , the kernel allocates the i th thread to pro-

cess the i th element of the N wavetables. This thread index-to-wavetable index mapping facilitates high data parallelism as the i th thread independently computes a single data point in the wavetable buffer $x_j[i]$ (see Fig. 4). For computing N time-varying tones, each thread computes $N L_d / L_s$ data points with a one thread index-to-multiple wavetable index mapping: the i th thread computes L_d / L_s wavetable elements $x_j[i \bmod L_s]$ in the N wavetables. This resource-intensive and on-the-fly computation of the chirped tone wavetables is performed at half-floating point precision in order to reduce latency, as high-frequency precision of the chirped tones isn't necessary for our application.

The WC kernel performs the vector additions (or subtractions if necessary) of the saved wavetables. The thread indices are mapped to wavetable indices in the same way as described in the WG kernel paragraph above. When the kernel is launched, the i th thread initializes a zero-valued float in one of its registers, and then iteratively adds or subtracts the values in the wavetables at index i to this register (see Fig. 4). This implementation accesses each data point in the wavetables only once, thus mitigating the latency associated with repetitive buffer accesses.

The WM kernel multiplexes the arbitrary waveform wavetables for the four DAC channels into a single buffer, which is transferred to the FIFO memory through RDMA in $4L_s$ -sized chunks (see Fig. 4). The data in the FIFO memory is read sequentially in groups of four in a single clock cycle. Each group contains the wavetable values for four DAC channels. The thread index to wavetable index mapping is also natural for the WM kernel. The i th thread takes the i th elements from each of the four wavetable buffers and arranges them sequentially as a group of four in the pinned memory buffer. Due to the simplicity of the kernel, it takes, on average, tens of microseconds to execute it and doesn't affect the program performance.

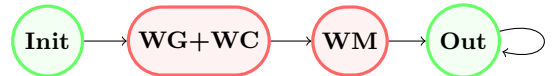


FIG. 5: The illustration of the kernel execution timeline in the static AWG pathway.

In practice, these kernels are modified to match the use case and merged together to minimize high-latency operations, such as repeatedly accessing the same chunk of data from DRAM memory. In the static AWG pathway, the kernels are launched sequentially (see Fig. 5). The WG and WC kernels are merged together to generate and store in memory all static (individual and summed) wavetables that will be reused in the dynamic pathways. Lastly, the WM reorganizes the data and saves it in the pinned memory buffer before it is transferred via RDMA to the DAC output channels for analog reconstruction.

In the Playback pathway (see Fig. 6), the WG and WC are also merged into a single kernel in order to compute

the entire dynamic waveform. Upon completion of the WG+WC kernel, the WM kernel reorders the dynamic waveform data before sending it over to the DAC output channels. This pathway ends in a static arbitrary waveform.

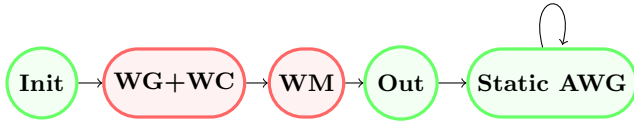


FIG. 6: The illustration of the kernel execution timeline in the Playback pathway.

In the Streaming pathway (see Fig. 7), the WG, WC, and WM are merged into a single kernel as new arbitrary waveform data is generated on the fly and streamed to the DAC output channels via RDMA.

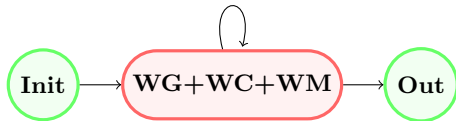


FIG. 7: The illustration of the kernel execution timeline in the Streaming pathway.

Lastly, shared memory usage can boost program performance. Shared memory is a programmer-controlled memory resource accessible to all threads in a block. In our implementation, shared memory stores temporary variables for dynamic waveform synthesis. However, its efficacy is limited due to infrequent data access in our case.

V. PERFORMANCE

Here we evaluate the performance of all the pathways—static and dynamic—that were implemented under the additive synthesis framework.

A. Static AWG pathway

We compare the time it takes for the Quadro RTX 6000 GPU (1.6 TFLOPS) versus the time it takes for the function generator widget on SBench6 6.5.4 build 21020 (the official software provided by the M4i.6622-x8 card vendor Spectrum Instrumentation) running on a CPU (AMD Ryzen 9 5950X 16-core processor) to compute the same static arbitrary waveforms. The function generator in SBench6 computes data in double precision (64 bits), but converts it to 16-bit data when it is replayed, as the DAC resolution is 16-bit.

In order to do this comparison, the SBench6 and the GPU perform the same calculation: Generate an arbitrary waveform of the form $a \sum_{j=0}^{N_{\text{static}}} \sin(2\pi(f_0 + j\Delta f)t)$

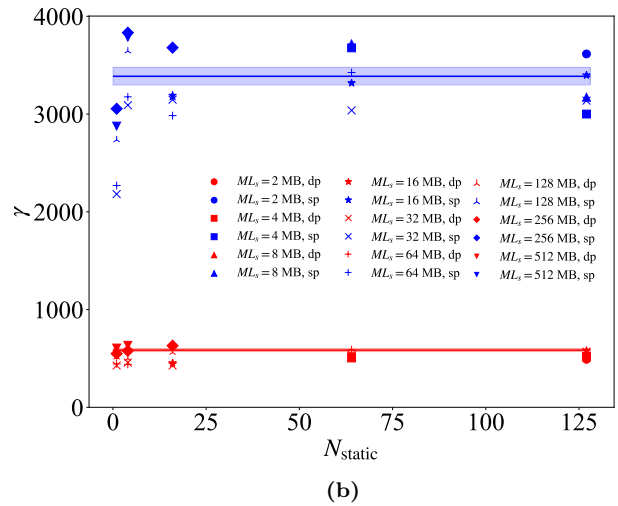
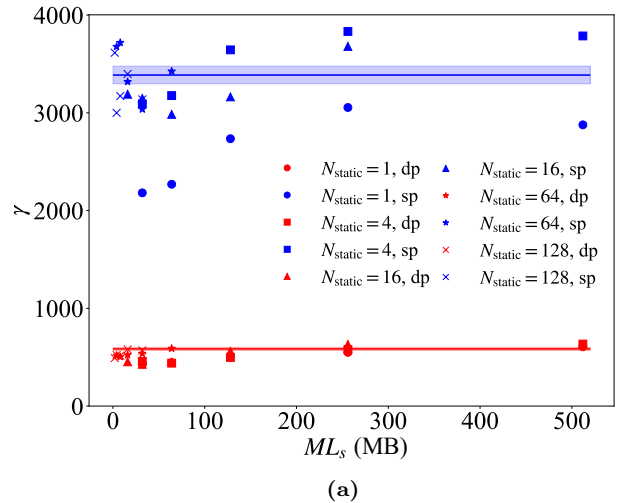


FIG. 8: The evaluation of the Static AWG pathway: The speedup ratios are $\gamma = C_1/C_{2,\text{sp}} = 3389_{-90}^{+92}$ and $\gamma = C_1/C_{2,\text{dp}} = 586_{-16}^{+16}$ for single-precision floating-point data computed on the GPU and double-precision floating-point data computed on the GPU respectively. The function generator in SBench6 computes data in double precision, but converts it to 16-bit data when it is replayed by the DAC. The data and the speedup ratio $\gamma = C_2/C_{1,\eta}$ are plotted as a function of (a) ML_s and (b) N_{static} .

of wavetable length ML_s , where M is a positive integer, $f_0 = 50$ MHz, and $\Delta f = 1$ MHz. We vary the wavetable length ML_s and the number of static single-frequency tones N_{static} and record the computation time $t_{\text{static},i}$. The GPU AWG computation time data is fit to the expression $t_{\text{static,GPU},\eta} = C_{1,\eta} N_{\text{static}}(ML_s)$ where $\eta = \text{sp}$ represents data computed in single floating-point precision, dp represents data computed in double floating-point precision. The SBench6 AWG computation data is fit to the expression $t_{\text{static,CPU}} = C_2 N_{\text{static}}(ML_s)$. The fitted results give $C_{1,\text{sp}} = 0.0126(1)$ ms/MB, $C_{1,\text{dp}} =$

0.0729(8) ms/MB, $C_2 = 42.7(7)$ ms/MB. Given these expressions, we define the speedup ratio (γ) as

$$\gamma = \frac{t_{\text{static,CPU}}}{t_{\text{static,GPU},\eta}} = \frac{C_2}{C_{1,\eta}}. \quad (11)$$

The speedup ratio is $\gamma = C_1/C_{2,\text{sp}} = 3389_{-90}^{+92}$ and $\gamma = C_1/C_{2,\text{dp}} = 586_{-16}^{+16}$ respectively. We plot the results of our measurements in Fig 8. The speedup ratio and the data are plotted as a function of ML_s in Fig. 8a and as a function of N_{static} in Fig. 8b. The speedup ratio γ is largely independent of these variables and clearly shows that the static AWG computation on the GPU outperforms the SBench6 computation by a few orders of magnitude in speed. The speedup ratio will further increase due to the higher complexity of the kernels, and more frequent and complicated memory access critical in implementing the dynamic AWG pathways. Additionally, SBench6 cannot perform on-the-fly computation of dynamic waveforms.

B. Dynamic AWG pathway: Streaming pathway

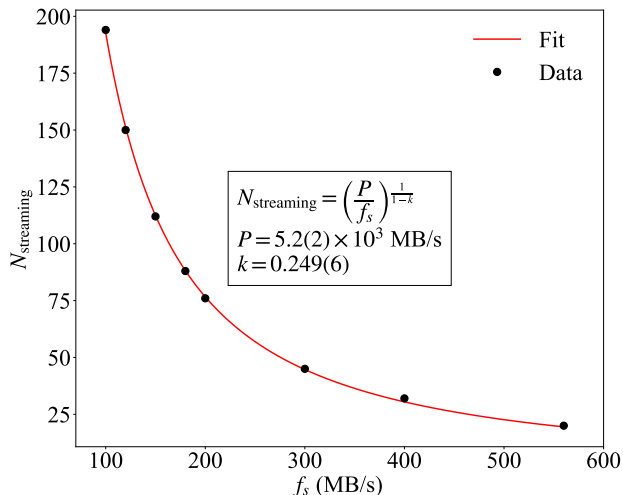


FIG. 9: Modeling the Streaming pathway: We plot the experimentally determined maximum number of tones $N_{\text{streaming}}$ that can be streamed as a function of the sample rate f_s . We also plot the fit to the data. R-squared of the fit is 0.9997.

In the Streaming pathway, each subsequent waveform chunk is evaluated in the time interval between the current and the upcoming RDMA transfers. In order to model the Streaming pathway, we compare the time it takes to transfer an L_s -sized chunk of data in the pinned memory buffer of the GPU to the FIFO memory and DAC via RDMA, to the time it takes for L_s -sized chunks of $N_{\text{streaming}}$ different tones to be computed in real-time, added together, and saved to the pinned memory buffer. It takes L_s/f_s amount of time to transfer an L_s -sized

chunk of data in the pinned memory buffer to the FIFO memory and the DAC via RDMA. On the other hand, the time it takes to generate an L_s -sized chunk of data representing the dynamic behaviour of $N_{\text{streaming}}$ time-varying tones is $N_{\text{streaming}}L_s/(PN_{\text{streaming}}^k) = N_{\text{streaming}}^{1-k}L_s/P$. Here $N_{\text{streaming}}L_s$ is the total number of samples that are computed and added together, and $PN_{\text{streaming}}^k$ is the rate at which this computation is performed. P is a constant pre-factor that has units of samples per second, and k is a dimensionless exponent that encapsulates the scaling dependence on the number of time-varying tones $N_{\text{streaming}}$. Equating the two times, we get the following expression for the number of tones that can be dynamically controlled and streamed ($N_{\text{streaming}}$) as a function of the sampling frequency (f_s):

$$N_{\text{streaming}} = \left(\frac{P}{f_s}\right)^{\frac{1}{1-k}} \quad (12)$$

Given a sampling rate f_s , we experimentally determine the maximum number of tones $N_{\text{streaming}}$ we can chirp indefinitely. We fit this data to the expression in Eq. 12. The R-squared value of the fit is 0.9997. We are able to chirp 20 tones at $f_s = 560$ MB/s, and 194 tones at $f_s = 100$ MB/s. With $k = 0.249$, the time it takes to compute $N_{\text{streaming}}$ tones increases sub-linearly: $N_{\text{streaming}}^{0.754}L_s/P$. This is because with more $N_{\text{streaming}}$ tones, more blocks are assigned to each SM on the GPU, which helps with the overall GPU throughput via latency hiding.

C. Dynamic AWG pathway: Playback pathway

In the Playback pathway, there's a latency between the start of the computation and when the DAC is ready to output the computed real-time arbitrary waveform. The latency depends on the number of time-varying tones N_{playback} and the length of the dynamic waveform Tf_s . Furthermore, the vector addition of N_{playback} time-varying tones scales as $t_{\text{overhead}}N_{\text{playback}}$. The Playback pathway computational latency (τ_{playback}) can be modelled as:

$$\tau_{\text{playback}} = A(Tf_s)^a N_{\text{playback}}^b + t_{\text{overhead}}N_{\text{playback}} \quad (13)$$

where A is a constant pre-factor; a, b are the dimensionless exponents that capture the scaling dependence on the length of dynamic waveform Tf_s and the number of time-varying tones N_{playback} respectively.

In our experiments, we set $f_s = 560$ MB/s. The latency τ_{playback} is extracted using a CPU timer synchronized with the GPU. We fit the data collected from varying N_{playback} and T independently to the two-dimensional model described in Eq. 13, as can be seen in Fig. 10a and Fig. 10b. In Fig. 10a, we plot the data alongside slices of the global fit along the N_{playback} axis. In Fig. 10b, we plot the data alongside slices of the global fit along the Tf_s axis. The R-squared value of the two-dimensional fit is 0.997. Both the exponents a and b are

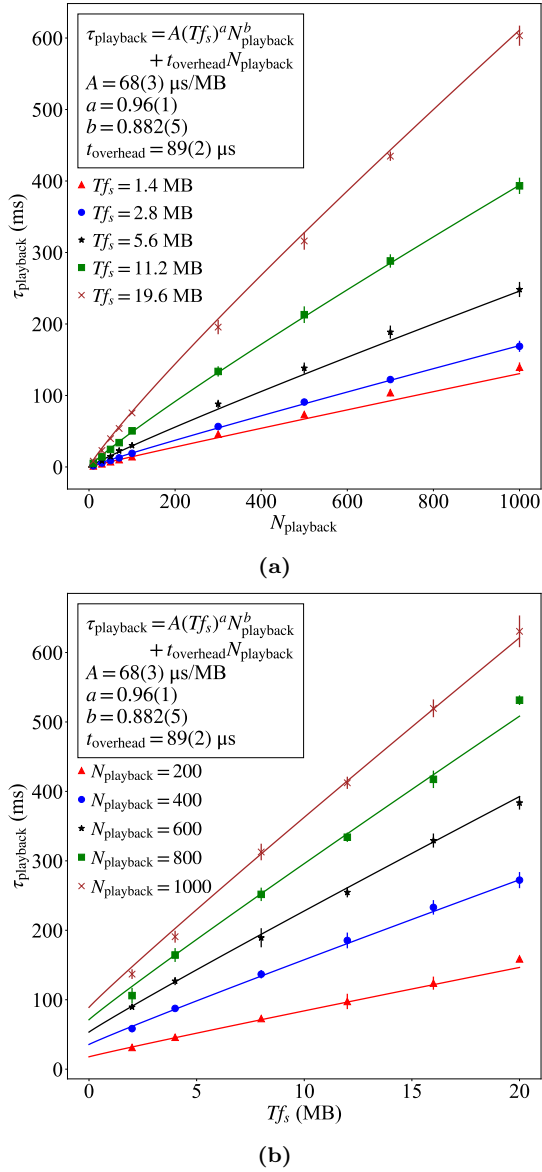


FIG. 10: Modelling the Playback pathway: The measured latency τ_{playback} data and slices of the global fit to the data are plotted as a function of (a) the number of chirped tones N_{playback} and (b) the length of the dynamic waveform Tf_s .

sub-linear. This suggests that with more N_{playback} tones and more considerable dynamic waveform lengths Tf_s , more blocks are assigned to each SM on the GPU, which helps with the overall GPU throughput via latency hiding.

Apart from the latency, another limitation inherent to the Playback pathway is the upper bound on the total memory ($N_{\text{playback}} Tf_s$ half-precision floating-point numbers) required by the pathway. This memory requirement must not exceed the GPU DRAM capacity. Given our GPU’s memory capacity of 24 GB, this imposes a constraint on the maximum number of tones that can be chirped, approximately limiting it to 1000 for a 35 ms

duration at a sample rate of 560 MB/s.

VI. SUMMARY AND OUTLOOK

In conclusion, we have implemented fast real-time arbitrary waveform generation on a GPU using the additive synthesis framework for waveform synthesis. We cast the additive synthesis framework as massively or “embarrassingly” data parallel and execute it efficiently on a GPU. We implement multiple pathways for arbitrary waveform generation: one static pathway, and two dynamic pathways. The static AWG pathway allows for the continuous generation of unmodulated arbitrary waveforms that are highly complex and precise. The choice of the dynamic AWG pathway depends on the application: generate a highly complex real-time arbitrary waveform for a short duration of time, or continuously stream a less complex real-time arbitrary waveform. Unlike FPGA-based systems, the system outlined in this paper only requires a commercial GPU and a commercial DAC module (M4i.6622-x8 in our case) that can be integrated into a desktop computer, and is developer-friendly for programmers with a background in C/C++. While this system was designed specifically for real-time rearrangement of stochastically loaded atoms in a large optical tweezer array into a defect-free array, it can be readily generalized and extended to other applications.

There are a few drawbacks in our implementation that can be improved in future updates. When we profile our implementations on NVIDIA Nsight, it states that the data transfer between DRAM memory and the caches limits the performance of the programs. So memory access patterns inside the GPU may be further optimized. Furthermore, the kernels access the buffers in a coalesced manner. However, the order in which they are accessed may not be optimal.

Multiple GPUs may be connected together via NVLink and NVSwitch to further accelerate the “embarrassingly” data parallel tasks like wavetable computation and vector addition under the additive synthesis framework. CUDA libraries like cuBLAS and cuFFT can be readily integrated into our code for more complex signal-processing tasks. Given that the speed of floating-point operations and the number of threads have been increasing steadily with every GPU generation, we expect the vector additions and the wavetable computations that comprise the additive synthesis framework to be even further accelerated in future GPU generations. Furthermore, the RDMA transfer to the DAC for waveform reconstruction could be improved with an interface that has greater speed and throughput than the PCIe 2.0 bus used in our setup. This would allow for higher Nyquist-limited frequencies to be synthesized. Finally, integrating a high-speed digitizer—capable of transferring sampled waveform data rapidly into GPU memory, via RDMA for instance—into our current arrangement could enable a simple yet complete real-time adaptive feedback control

over arbitrary waveforms.

VII. CRediT AUTHOR STATEMENT

Juntian Tu: Software, Investigation, Validation, Formal analysis, Data Curation, Writing, Visualization.
Sarthak Subhankar: Conceptualization, Methodology, Supervision, Formal analysis, Data Curation, Resources, Writing, Visualization, Project administration.

VIII. ACKNOWLEDGEMENTS

We thank Alessandro Restelli, Sayantan Sarkar, and Alexander Craddock for carefully reading the manuscript. We thank Office of Naval Research (Grant No. N000142212085) National Science Foundation (QLCI grant OMA-2120757) for funding this project.

-
- [1] D. Creasey, *Audio Processes* (Routledge, 2016).
- [2] C. Roads, *The Computer Music Tutorial, Second Edition* (The MIT Press, 2023).
- [3] J. Lin, F. T. Liang, Y. Xu, L. H. Sun, C. Guo, S. K. Liao, and C. Z. Peng, Scalable and customizable arbitrary waveform generator for superconducting quantum computing, *AIP Advances* **9**, 115309 (2019).
- [4] Y. Yang, Z. Shen, X. Zhu, C. Deng, S. Liu, and Q. An, An fpga-based low latency awg for superconducting quantum computers, in *2021 IEEE International Instrumentation and Measurement Technology Conference (I2MTC)* (2021) pp. 1–6.
- [5] L. Stefanazzi, K. Treptow, N. Wilcer, C. Stoughton, C. Bradford, S. Uemura, S. Zorzetti, S. Montella, G. Canceledo, S. Sussman, A. Houck, S. Saxena, H. Arnaldi, A. Agrawal, H. Zhang, C. Ding, and D. I. Schuster, The QICK (Quantum Instrumentation Control Kit): Read-out and control for qubits and detectors, *Review of Scientific Instruments* **93**, 044709 (2022).
- [6] M. Endres, H. Bernien, A. Keesling, H. Levine, E. R. Anschuetz, A. Krajenbrink, C. Senko, V. Vuletic, M. Greiner, and M. D. Lukin, Atom-by-atom assembly of defect-free one-dimensional cold atom arrays, *Science* **354**, 1024 (2016).
- [7] D. Barredo, S. de Léséleuc, V. Lienhard, T. Lahaye, and A. Browaeys, An atom-by-atom assembler of defect-free arbitrary two-dimensional atomic arrays, *Science* **354**, 1021 (2016).
- [8] L. Anderegg, L. W. Cheuk, Y. Bao, S. Burchesky, W. Ketterle, K.-K. Ni, and J. M. Doyle, An optical tweezer array of ultracold molecules, *Science* **365**, 1156 (2019).
- [9] I. S. Madjarov, *Entangling, Controlling, and Detecting Individual Strontium Atoms in Optical Tweezer Arrays*, Theses, California Institute of Technology (2021), available at https://thesis.library.caltech.edu/14061/7/Thesis_Ivaylo_Madjarov.pdf.
- [10] H. J. Levine, *Quantum Information Processing and Quantum Simulation with Programmable Rydberg Atom Arrays*, Ph.D. thesis, Harvard University (2021), available at <https://nrs.harvard.edu/URN-3:HUL.INSTREPOS:37368420>.
- [11] Avionics Department Code, 450000E, *Electronic Warfare and Radar Systems Engineering Handbook*, 4th ed. (NAWCWD Technical Communication Office, POINT MUGU, CA, 2013) available at <https://apps.dtic.mil/sti/citations/ADA617071>.
- [12] H. H. Gatzert, V. Saile, and J. Leuthold, Lithography, in *Micro and Nano Fabrication: Tools and Processes* (Springer Berlin Heidelberg, Berlin, Heidelberg, 2015) pp. 313–395.
- [13] M. R. Bales and S. C. Sutphin, Fpga architecture for real-time wideband waveform synthesis, in *2015 IEEE Radar Conference (RadarCon)* (2015) pp. 0605–0610.
- [14] T. Alpert, M. Werz, F. Lang, D. Ferenci, M. Masini, M. Groezing, and M. Berroth, Arbitrary waveform generator based on fpga and high-speed dac with real-time interface, in *PRIME 2012; 8th Conference on Ph.D. Research in Microelectronics & Electronics* (2012) pp. 1–4.
- [15] M. Yearly, R. Fink, D. Beck, D. Guidry, and M. Burns, A dsp-based mixed-signal waveform generator, *IEEE Transactions on Instrumentation and Measurement* **53**, 665 (2004).
- [16] S. Prasad and S. Sanyal, Design of arbitrary waveform generator based on direct digital synthesis technique using code composer studio platform, in *2007 International Symposium on Signals, Circuits and Systems*, Vol. 1 (2007) pp. 1–4.
- [17] A. HajiRassouliha, A. J. Taberner, M. P. Nash, and P. M. Nielsen, Suitability of recent hardware accelerators (dps, fpgas, and gpus) for computer vision and image processing algorithms, *Signal Processing: Image Communication* **68**, 101 (2018).
- [18] P. Symons, *Digital Waveform Generation* (Cambridge University Press, 2013).
- [19] *CUDA C++ Programming Guide*, NVIDIA (2024), available at https://docs.nvidia.com/cuda/pdf/CUDA_C_Programming_Guide.pdf.
- [20] J. Cheng, M. Grossman, and T. McKercher, *Professional CUDA® C programming* (John Wiley & Sons, Inc., 2014).
- [21] D. B. Kirk and W. mei W. Hwu, *Programming Massively Parallel Processors: A Hands-on Approach* (Elsevier Inc., 2010).
- [22] K. Fatahalian and M. Houston, Gpus: A closer look: As the line between gpu and cpus begins to blur, it's important to understand what makes gpu tick., *Queue* **6**, 18–28 (2008).
- [23] E. Lindholm, J. Nickolls, S. Oberman, and J. Montrym, Nvidia tesla: A unified graphics and computing architecture, *IEEE Micro* **28**, 39 (2008).
- [24] R. S. Perdana, B. Sitohang, and A. B. Suksmono, A survey of graphics processing unit (GPU) utilization for radar signal and data processing system, *Proceedings of the 2017 6th International Conference on Electrical En-*

- gineering and Informatics: Sustainable Society Through Digital Innovation, ICEEI 2017 **2017-Novem**, 1 (2017).
- [25] J. Cong, Z. Fang, M. Lo, H. Wang, J. Xu, and S. Zhang, Understanding Performance Differences of FPGAs and GPUs, Proceedings - 26th IEEE International Symposium on Field-Programmable Custom Computing Machines, FCCM 2018 , 93 (2018).
- [26] J. A. Wilson and J. Williams, Massively parallel signal processing using the graphics processing unit for real-time brain-computer interface feature extraction, Frontiers in Neuroengineering **2**, (2009).
- [27] P. Pawlowski, A. Dabrowski, M. Stankiewicz, and F. Misiorek, Fast and accurate digital signal processing realized with gpgpu technology, Przegląd Elektrotechniczny **88**, 47 (2012).
- [28] J. A. Belloch, B. Bank, L. Savioja, A. Gonzalez, and V. Välimäki, Multi-channel iir filtering of audio signals using a gpu, in *2014 IEEE International Conference on Acoustics, Speech and Signal Processing (ICASSP)* (2014) pp. 6692–6696.
- [29] M. D. Mccool, Signal processing and general-purpose computing and gpus [exploratory dsp], IEEE Signal Processing Magazine **24**, 109 (2007).
- [30] W. Plishker, G. F. Zaki, S. S. Bhattacharyya, C. Clancy, and J. Kuykendall, Applying graphics processor acceleration in a software defined radio prototyping environment, in *2011 22nd IEEE International Symposium on Rapid System Prototyping* (2011) pp. 67–73.
- [31] K. Li, M. Wu, G. Wang, and J. R. Cavallaro, A high performance gpu-based software-defined basestation, in *2014 48th Asilomar Conference on Signals, Systems and Computers* (2014) pp. 2060–2064.
- [32] R. Akeela and B. Dezfouli, Software-defined radios: Architecture, state-of-the-art, and challenges, Computer Communications **128**, 106 (2018).
- [33] C. M. Holland, Y. Lu, and L. W. Cheuk, On-demand entanglement of molecules in a reconfigurable optical tweezer array, Science **382**, 1143 (2023).
- [34] D. Bluvstein, S. J. Evered, A. A. Geim, S. H. Li, H. Zhou, T. Manovitz, S. Ebadi, M. Cain, M. Kalinowski, D. Hangleiter, J. P. Bonilla Ataides, N. Maskara, I. Cong, X. Gao, P. Sales Rodriguez, T. Karolyshyn, G. Semeghini, M. J. Gullans, M. Greiner, V. Vuletić, and M. D. Lukin, Logical quantum processor based on reconfigurable atom arrays, Nature **626**, 58 (2024).
- [35] Y. Bao, S. S. Yu, L. Anderegg, E. Chae, W. Ketterle, K. K. Ni, and J. M. Doyle, Dipolar spin-exchange and entanglement between molecules in an optical tweezer array, Science **382**, 1138 (2023).
- [36] A. Keesling, A. Omran, H. Levine, H. Bernien, H. Pichler, S. Choi, R. Samajdar, S. Schwartz, P. Silvi, S. Sachdev, P. Zoller, M. Endres, M. Greiner, V. Vuletić, and M. D. Lukin, Quantum Kibble–Zurek mechanism and critical dynamics on a programmable Rydberg simulator, Nature **568**, 207 (2019), arXiv:1809.05540.
- [37] W. J. Eckner, N. Darkwah Oppong, A. Cao, A. W. Young, W. R. Milner, J. M. Robinson, J. Ye, and A. M. Kaufman, Realizing spin squeezing with Rydberg interactions in an optical clock, Nature **621**, 734 (2023).
- [38] G. Bornet, G. Emperauger, C. Chen, B. Ye, M. Block, M. Bintz, J. A. Boyd, D. Barredo, T. Comparin, F. Mezzacapo, T. Roscilde, T. Lahaye, N. Y. Yao, and A. Browaeys, Scalable spin squeezing in a dipolar Rydberg atom array, Nature **621**, 728 (2023), arXiv:2303.08053.
- [39] Y. H. Fung, P. Sompert, and M. F. Andersen, Single Atoms Preparation Using Light-Assisted Collisions, Technologies **4**, 4 (2016).
- [40] N. Schlosser, G. Reymond, I. Protsenko, and P. Grangier, Sub-poissonian loading of single atoms in a microscopic dipole trap, Nature **411**, 1024 (2001).
- [41] N. Schlosser, G. Reymond, and P. Grangier, Collisional Blockade in Microscopic Optical Dipole Traps, Physical Review Letters **89**, 1 (2002).
- [42] M. O. Brown, T. Thiele, C. Kiehl, T. W. Hsu, and C. A. Regal, Gray-Molasses Optical-Tweezer Loading: Controlling Collisions for Scaling Atom-Array Assembly, Physical Review X **9**, 11057 (2019), arXiv:1811.01448.
- [43] K.-N. Schymik, *Scaling-up the Tweezer Platform - Trapping Arrays of Single Atoms in a Cryogenic Environment*, Theses, Université Paris-Saclay (2022), available at https://pastel.hal.science/tel-03643133/file/105658_SCHYMIK_2022_archivage.pdf.
- [44] Y. Shibasaki, K. Asami, R. Aoki, A. Hatta, A. Kuwana, and H. Kobayashi, Analysis and design of multi-tone signal generation algorithms for reducing crest factor, in *2020 IEEE 29th Asian Test Symposium (ATS)* (2020) pp. 1–6.
- [45] M. Russ, Chapter 3 - making sounds with analogue electronics, in *Sound Synthesis and Sampling (Third Edition)*, Music Technology, edited by M. Russ (Focal Press, Oxford, 2009) third edition ed., pp. 99–204.
- [46] *A technical tutorial on digital signal synthesis*, Analog Devices (1999), available at <http://www.ieee.li/pdf/essay/dds.pdf>.
- [47] H. Yang, S.-B. Ryu, H.-C. Lee, S.-G. Lee, S.-S. Yong, and J.-H. Kim, Implementation of dds chirp signal generator on fpga, in *2014 International Conference on Information and Communication Technology Convergence (ICTC)* (2014) pp. 956–959.
- [48] Nicholas Wilt, *The CUDA Handbook: A Comprehensive Guide to GPU Programming* (Addison-Wesley, 2013) available at <https://www.cudahandbook.com/>.
- [49] S. Cook, *CUDA Programming: A Developer's Guide to Parallel Computing with GPUs* (Morgan Kaufmann, 2012) pp. 1–576.
- [50] L. Cordesses, Direct digital synthesis: A tool for periodic wave generation (Part 1), IEEE Signal Processing Magazine **21**, 50 (2004).
- [51] M. Schroeder, Synthesis of low-peak-factor signals and binary sequences with low autocorrelation (corresp.), IEEE Transactions on Information Theory **16**, 85 (1970).
- [52] S. Spence, R. V. Brooks, D. K. Ruttley, A. Guttridge, and S. L. Cornish, Preparation of 87rb and 133cs in the motional ground state of a single optical tweezer, New Journal of Physics **24**, 103022 (2022).
- [53] L. R. Liu, J. D. Hood, Y. Yu, J. T. Zhang, K. Wang, Y. W. Lin, T. Rosenband, and K. K. Ni, Molecular assembly of ground-state cooled single atoms, Physical Review X **9**, 021039 (2019).
- [54] *CUDA C++ Best Practices Guide*, NVIDIA (2023), available at https://docs.nvidia.com/cuda/pdf/CUDA_C_Best_Practices_Guide.pdf.

Appendix: Parallel computation optimization

We primarily consulted NVIDIA’s CUDA C++ Programming Guide[19] and CUDA C++ Best Practices Guide [54] to enhance computational efficiency. In our implementations, we aimed to minimize computational latencies during the real-time waveform output. In fact, we tried to move all the long latency operations to the initialization state.

- To circumvent bulky data transfers between the GPU and CPU, we allocate all data buffers in GPU memory and reuse temporary data, thus alleviating constraints imposed by PCIe bus bandwidth. All synthesis parameters are transmitted from the CPU to the GPU only during initialization or when static arbitrary waveforms are being reconstructed. This is because the GPU is idle in these states. Besides sending parameters, the CPU exclusively interacts with the GPU when launching CUDA kernel functions.
- We store pre-calculated and reusable data in GPU DRAM, such as wavetables, prior to additive synthesis. This offloads computationally intensive tasks to the initialization stage, mitigating the need for repeating computations, which helps reduce latency.
- Computing the sine of a large number can incur significant computational cost, especially when processing sample data with a large position index i .

To alleviate this problem, we apply a `modf()` to the phase $\phi[i]$ before executing any trigonometric operations:

$$V[i] = \sum_j a_j \sin \left[2\pi \times \mathbf{modf} \left(\frac{\phi_j[i]}{2\pi} \right) \right] \quad (14)$$

- We use low-precision data types for real-time/dynamic waveform generation. The SFUs on the GPU are capable of very fast execution of special floating-point arithmetic functions called intrinsic functions. However, the SFU can only evaluate intrinsic functions at single-float precision or lower. Moreover, current GPUs are optimized to process vector structures such as float2 vectors or half2 vectors. Given our specific requirement of chirping tones to move optical tweezers using AODs, which do not necessitate high precision, we utilize half2 structures in conjunction with intrinsic functions to speed up the computation.
- We use fused multiply-add (FMA) operations and `_restrict_` qualifier to further improve code performance. The `_restrict_` keyword declares an array argument of a kernel function to be unaliased, which means the array is only accessible through a single symbol in the scope of the executing kernel. This allows for additional optimization during compilation. Given that our kernels access data in the buffers only once, most arrays in our program benefit from this optimization.